ACS Synthetic Biology
Cite This: ACS Synth. Biol. 2018, 7, 2765−2774
Letter
pubs.acs.org/synthbio

An *in Vivo* Binding Assay for RNA-Binding Proteins Based on Repression of a Reporter Gene

Noa Katz,[†,#] Roni Cohen,[†,#] Oz Solomon,[†,§] Beate Kaufmann,[†] Orna Atar,[†] Zohar Yakhini,[‡,§] Sarah Goldberg,[†] and Roee Amit*[,†,∥]

[†]Department of Biotechnology and Food Engineering, Technion − Israel Institute of Technology, Haifa 32000, Israel
[‡]Department of Computer Science, Technion − Israel Institute of Technology, Haifa 32000, Israel
[§]School of Computer Science, Interdisciplinary Center, Herzeliya 46150, Israel
[∥]Russell Berrie Nanotechnology Institute, Technion − Israel Institute of Technology, Haifa 32000, Israel

Supporting Information

ABSTRACT: We study translation repression in bacteria by engineering a regulatory circuit that functions as a binding assay for RNA binding proteins (RBP) *in vivo*. We do so by inducing expression of a fluorescent protein−RBP chimera, together with encoding its binding site at various positions within the ribosomal initiation region (+11−13 nt from the AUG) of a reporter module. We show that when bound by their cognate RBPs, the phage coat proteins for PP7 (PCP) and Qβ (QCP), strong repression is observed for all hairpin positions within the initiation region. Yet, a sharp transition to no-effect is observed when positioned in the elongation region, at a single-nucleotide resolution. Employing *in vivo* Selective 2′-hydroxyl acylation analyzed by primer extension followed by sequencing (SHAPE-seq) for a representative construct, established that in the translationally active state the mRNA molecule is nonstructured, while in the repressed state a structured signature was detected. We then utilize this regulatory phenomena to quantify the binding affinity of the coat proteins of phages MS2, PP7, GA, and Qβ to 14 cognate and noncognate binding sites *in vivo*. Using our circuit, we demonstrate qualitative differences between *in vitro* to *in vivo* binding characteristics for various variants when comparing to past studies. Furthermore, by introducing a simple mutation to the loop region for the Qβ-wt site, MCP binding is abolished, creating the first high-affinity QCP site that is completely orthogonal to MCP. Consequently, we demonstrate that our hybrid transcriptional−post-transcriptional circuit can be utilized as a binding assay to quantify RNA−RBP interactions *in vivo*.

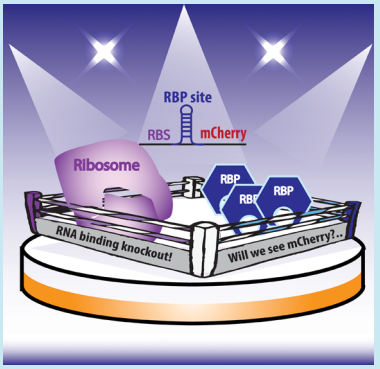

KEYWORDS: *RNA binding protein (RBP), MS2, PP7, phage coat protein, binding assay, post-transcriptional regulation, SHAPE-seq, translation repression, synthetic circuit*

In bacteria, post-transcriptional regulation has been studied extensively in recent decades. There are well-documented examples of RBPs that either inhibit or directly compete with ribosome binding. RNA hairpins have been studied in three distinct positions: either immediately downstream of the AUG,[1] upstream of the Shine−Dalgarno sequence,[2] or as structures that entrap Shine−Dalgarno motifs, as is the case for the PP7 and MS2 phage coat-protein binding sites. While these studies indicate a richness of RBP−RNA-based regulatory mechanisms, a systematic understanding of the relationship between RBP binding, sequence specificity, the underlying secondary and tertiary RNA structure, and the resulting regulatory output is still lacking.

In recent years, advances in next generation sequencing (NGS) technology combined with selective nucleic acid probing approaches have facilitated focused study of specific RNA structures *in vivo*. These chemical-modification approaches[3−7] can generate a "footprint" of the dynamical structure of a chosen RNA molecule *in vivo*, while in complex with ribosomes and/or other RBPs. In parallel, synthetic biology approaches that simultaneously characterize large libraries of synthetic regulatory constructs have been increasingly used to complement the detailed study of single mRNA transcripts. While these synthetic approaches have been mostly applied to characterizing parts that regulate transcription,[8−11] their potential for deciphering post-transcriptional regulatory mechanisms have been demonstrated in a recent study that interrogated IRES sequences in mammalian cells.[12]

Building on these advances and on the development of a translational repression circuit that was used to characterize the binding characteristics of the RBP L7Ae in both bacteria and mammalian cells,[13] we engineering a hybrid transcriptional−post-transcription circuit that was designed to be a general platform for characterizing RBP binding *in vivo*. Using the circuit, we measured the regulatory output of a small library of synthetic constructs in which we systematically varied the

Received: September 10, 2018
Published: November 8, 2018

DOI: 10.1021/acssynbio.8b00378
ACS Synth. Biol. 2018, 7, 2765−2774

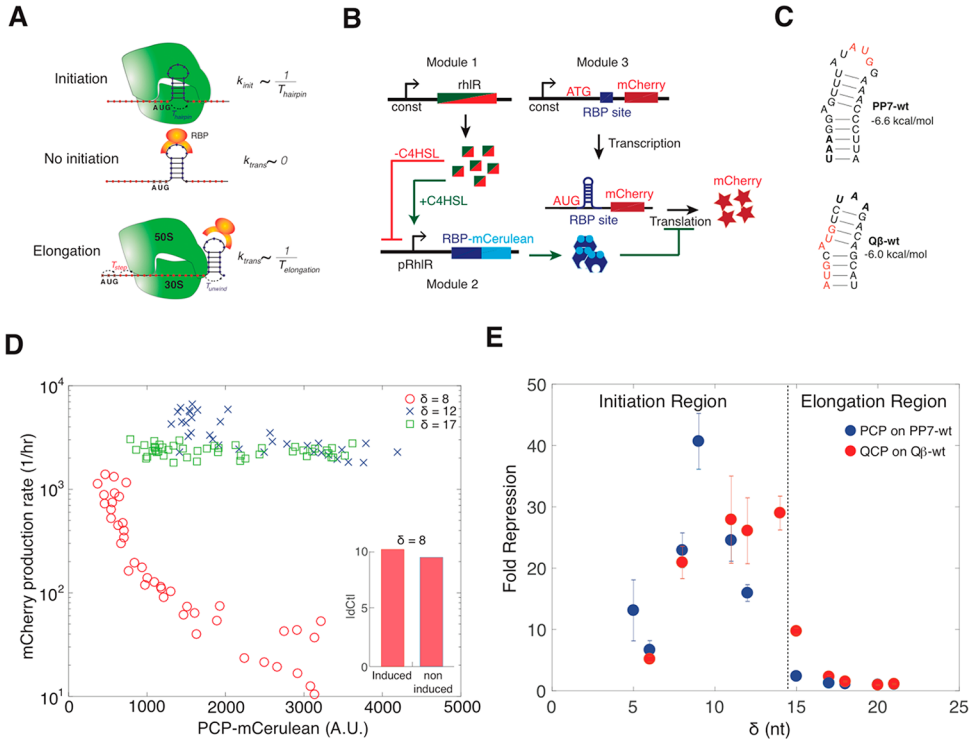

Figure 1. Translational regulation by a RBP-hairpin complex in the ribosomal initiation region. (A) A schematic for the hypothesized repression mechanism. The position of the hairpin within the ribosomal initiation region dictates the rate initiation $T_{hairpin}$, which in turn may control the rate of translation (top). When bound by an RBP (middle) the hairpin−RBP complex is able to disrupt initiation, thus inhibiting translation. If the hairpin is positioned downstream of the initiation region (bottom), initiation and subsequent elongation is likely to occur, leading to unwinding of the RBP-hairpin complex by the ribosome. (B) Gene regulatory circuit: (left-top) transducer plasmid−module 1: rhlR expression cassette; (left-bottom) transducer plasmid−module 2: RBP-mCerulean expression cassette under the control of pRhlR; (right-top) reporter plasmid−module 3: mCherry reporter expression under the control of a constitutive promoter; and (right-bottom) resultant mRNA encoding a folded RBP binding site with the ribosomal initiation region. When the binding site is occupied by the RBP, translation repression ensues. (C) The two hairpins used in this experiment were the native (wt) binding sites for the PP7and Qβ coat proteins. Stop codons and start codons inside the binding sites are highlighted, in bold and red. Note, positions where stop codons are in-frame were not tested, and so are most of the start codons. For those start codons that are in-frame—Qb at the second position in each frame—no different response was generated compared with the other strains, supporting a lack of detectable effect for the second in-frame AUG. (D) Dose−response functions for PCP with a reporter mRNA encoding PP7-wt at three positions: δ = 8 (red), δ = 12 (blue), and δ = 17 (green) nt. Inset: quantitative RT-PCR results for mRNA levels for the PP7-wt δ = 8 with and without induction. (E) Fold-repression measurements for PCP (blue) and QCP (red) as a function of hairpin position δ. Fold repression is computed by the ratio of the mCherry rate of production at no induction to the rate of production at full induction. Note, for three constructs (PCP with δ = 14, and QCP with δ = 5 and δ = 9) the basal levels without induction were too low for fold-repression measurements.

position and type of RBP binding sites. In addition, we applied Selective 2′-hydroxyl acylation analyzed by primer extension sequencing (SHAPE-seq)[14,15,6] to a single variant, to further characterize RBP-based regulatory mechanisms in bacteria. Our findings indicate that the chosen hairpin-binding RBPs (coat proteins from the bacteriophages GA,[16] MS2,[17] PP7,[18] and Qβ[19]), generate a strong repression response when bound to the translation initiation region. This inhibitory response is associated with RNA-restructuring that spans a large segment of the RNA, including both the RBP binding site and the RBS. We employed this strong repression phenomenon as an *in vivo* binding assay for RBP−RNA interactions. Using our synthetic regulatory circuit as a binding assay, we quantitatively characterized RBP binding affinity to a set of mutated binding sites in a high-throughput manner, thereby increasing our understanding of RBP−RNA binding *in vivo* and enabling the engineering of more complex RNA-based applications.

RESULTS AND DISCUSSION

RBPs Repress Translation When Bound within δ < 15 from the AUG. We hypothesized (Figure 1A) that a hairpin may be tolerated within the ribosomal initiation region facilitating translation if sufficiently unstable, but once bound by an RBP, initiation will be inhibited leading to a translational repression effect. To test this hypothesis, we designed a trimodule transcriptional and post-transcriptional gene regulatory circuit that was encoded on two plasmids (transducing and reporting) that were simultaneously transformed into *E. coli* (Figure 1B). The transducing plasmid (Figure 1B-top) encoded a rhlR gene under the control of a constitutive promoter on the first module, and either the phage coat protein for PP7 (PCP) or Qβ (QCP) fused to mCerulean, under the control of a pRhlR promoter inducible by *N*-butanoyl-L-homoserine lactone (C_4−HSL) on the second module. The reporter plasmid initially encoded the two wild-type binding sites (PP7-wt and Qβ-wt) for PCP and QCP at several positions downstream to the AUG of an *mCherry* reporter gene. The two native binding sites (Figure 1C) are characterized by hairpins of a varying length, which are interrupted by a single unpaired nucleotide or "bulge", and comprise a loop of either size 3 nt (Qβ-wt) or 6 nucleotides (PP7-wt). We constructed 12 variants for each binding site

DOI: 10.1021/acssynbio.8b00378
ACS Synth. Biol. 2018, 7, 2765−2774

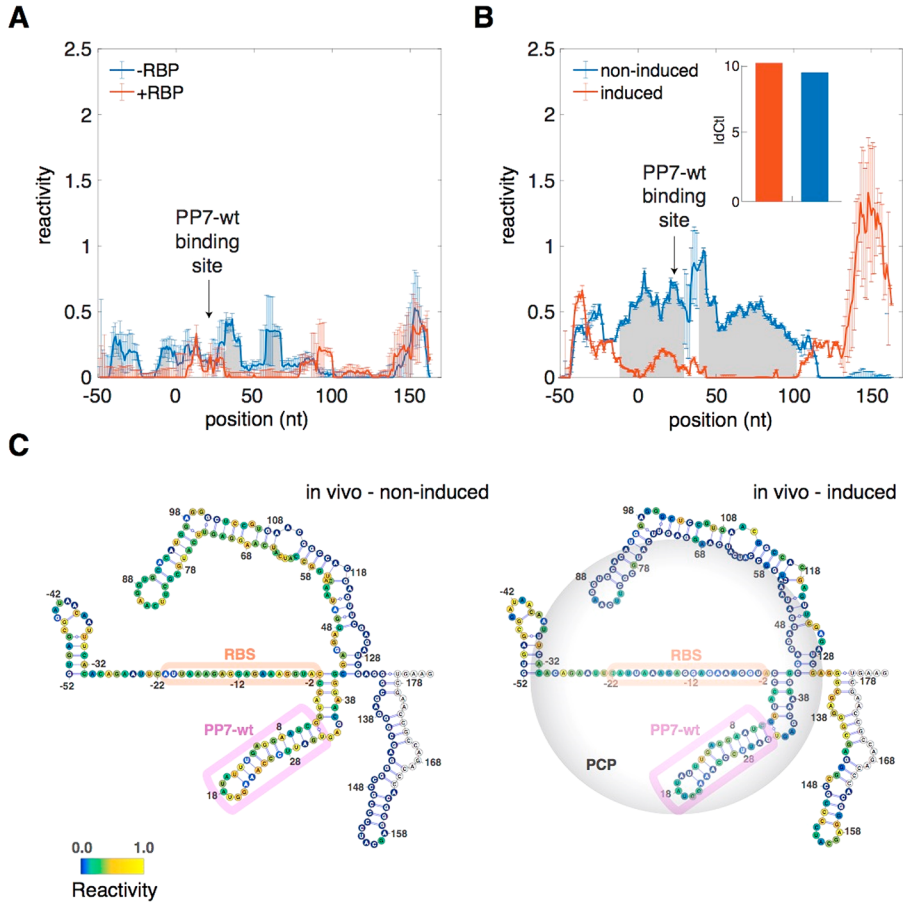

Figure 2. SHAPE-seq analysis of the PP7-wt binding site in the absence and in the presence of RBP. (A) *In vitro* reactivity. Scores for the SHAPE-seq reactions carried out on refolded mCherry reporter mRNA molecules containing a PP7-wt binding site at $\delta = 6$ with (red) and without (blue) a recombinant PCP present in the reaction buffer. (B) *In vivo* reactivity. Scores for the SHAPE-seq reactions carried out *in vivo* on the PP7-wt $\delta = 6$ construct with the PCP-mCerulean protein noninduced (blue) or induced (red). For both A and B panels, gray shades signify segments of RNA where a statistically significant difference in reactivity scores (as computed by a *Z*-factor analysis) was detected between the +RBP and −RBP (A), and induced and noninduced (B) cases, respectively. Error bars were computed using boot-strap resampling and subsequent averaging over two biological replicates. See also Figure S4 and associated discussion for comparison of results using our reactivity definition with another reactivity analysis using a model-based approach. (C) Structural schematics of the segment of the PP7-wt $\delta = 6$ construct that was subjected to SHAPE-seq *in vitro*. The structures are overlaid by the reactivity scores (represented as heatmaps from blue, low reactivity, to yellow, high reactivity) for the noninduced (left) and induced (right) cases, respectively. Binding site and RBS are highlighted magenta and orange ovals, respectively. Gray circle in right structure corresponds to the range of protection by a bound RBP. Noncolored bases correspond to position of the reverse transcriptase primer.

type starting at $\delta = 5$ exploring every single position until $\delta = 21$, except for those where an internal hairpin stop codon and most of the internal start codons were in frame (see note in figure caption). Each transducer−reporter plasmid pair was transformed into *E. coli* TOP10 and grown in 24 different C_4−HSL concentrations, in duplicate. Optical density, mCherry, and mCerulean fluorescence levels were measured at multiple time points for each inducer concentration. From these data, mCherry production rates[20,21] were computed over a 2−3 h window (see Supporting Methods and Figure S1) for each inducer level, and mCerulean levels were averaged over the same time frames. In Figure 1D we plot a series of dose−response curves obtained for PCP on three constructs containing the PP7-wt binding site, positioned at $\delta = 8$ (red), 12 (blue), and 17 (green) nt. To first rule out that the repression response stems from different number of RNA transcripts or degradation-related effects, we checked that the RNA levels at both states were similar using quantitative real-time PCR (Figure 1D-inset). For the hairpin located at $\delta = 8$, the mCherry production rate is reduced by nearly 2 orders of magnitude as a function of RBP concentration, while the hairpin positioned at $\delta = 12$ produced a weakly repressing dose−response function, and no RBP-induced repression was observed at $\delta = 17$.

Next, we computed the fold repression, defined as the ratio of mCherry production rate at no induction to full induction (*i.e.*, low to high mCerulean fluorescence levels), measured for the PCP on PP7-wt constructs. We plot the results for PCP in Figure 1E (blue circles). The figure shows that strong repression is triggered by PCP induction for all available positions in the region demarked by $\delta < 15$ (dashed line). However, fold repression by PCP rapidly diminishes for $\delta \geq 15$, and seems to disappear for $\delta \geq 17$ positions for all constructs. To show that this repression phenomenon was not limited to the PCP−PP7-wt interaction, we tested the translation repression effect generated by the QCP-mCerulean protein when induced in the presence of a reporter gene encoding the Qβ-wt binding site at various positions. We plot

DOI: 10.1021/acssynbio.8b00378
ACS Synth. Biol. 2018, 7, 2765−2774

the results for the QCP-induced fold repression in Figure 1E (red). The results show a similar fold-repression response behavior for QCP to that observed for PCP with strong repression observed for $\delta < 15$, and a rapid decline for $\delta > 15$ positions. Consequently, our data indicates that the region immediately downstream to the AUG and up to $\delta \sim 15$ seems to be susceptible to interference with translation making it a "hot spot" for potential translational repression mechanisms.

***In Vitro* SHAPE-seq Reveal an Extended Protected Region by PCP.** To provide a structural perspective on the inhibition mechanism triggered by the RBP binding to their hairpin binding sites, we employed SHAPE-seq. Specifically, we used acylimidazole reagent 2-methylnicotinic acid imidazolide (NAI), which modifies the 2′ OH of non- or less-structured, accessible RNA nucleotides as found in single-stranded RNA molecules.[14] We hypothesized that SHAPE-Seq data can provide a protection footprint (as in Smola *et al.*[22]) that develops when the RBP is bound to its cognate binding site. SHAPE-seq is a next generation sequencing approach (see Materials and Methods and Figure S2 for details), whereby an insight into the structure of an mRNA molecule can be obtained *via* selective modification of "unprotected" RNA segments. "Unprotected" segments mean single-stranded nucleotides that do not participate in any form of interaction, such as Watson−Crick base-pairing and RBP-based interactions. These modifications cause the reverse transcriptase to stall and fall off the RNA strand, leading to a pool of cDNA molecules at varying lengths. Therefore, by counting the number of reads that end in positions along the molecule we can directly measure the number of molecules within this length and can estimate the propensity of this RNA base to be unbound (*i.e.*, single-stranded). The single nucleotide propensity for modification is then calculated to a value that is referred to as "reactivity" score, which is computed from the ratio of the normalized modified to unmodified read count (see Supporting Information for details).

In our version of the reactivity score, any negative values are set to 0, indicating that the nucleotides at those particular positions do not get modified. We used boot-strapping statistics (as in refs 23, 24) and *Z*-factor analysis (as in refs 22, 25, 26; see Supporting Information for definition) to identify the regions on the RNA molecule where the observed differences between the signals at +RBP and −RBP are statistically significant (equal to or more than three sigmas). Finally, to eliminate method bias, we repeated the reactivity analysis on all our data sets using a model-based analysis approach.[23,24] In all cases studied the reactivity results from both methods being in good agreement (see Figure S4 and associated discussion).

In Figure 2A, we present the results for the reactivity analysis carried out on the *in vitro* SHAPE-seq data for the PP7-wt $\delta = 6$ construct with (red line, +RBP) and without (blue line, −RBP) the presence of a recombinant PCP protein in the reaction solution. Reactivities are presented as a running average over a 10 nt window to eliminate high frequency noise (for further details about the analysis pipeline, see Supporting Information and Figure S3). The *in vitro* modification experiments were carried out after refolding of the RNA followed by 30 min incubation at 37 °C with or without the recombinant PCP, and subsequently modified by the SHAPE reagent (*i.e.*, NAI). The plot shows that for the −RBP case (blue line) the reactivity pattern is a varying function of nucleotide position, reflecting a footprint of some underlying structure. Namely, the segments that are reactive (*e.g.*, −20 to 40 nt range), and those which are not (*e.g.*, 110−140 nt range), indicate noninteracting and highly sequestered nucleotides, respectively.

With the addition of the RBP (red line), the reactivity level in the −50 to 80 nt range is predominantly 0. This indicates that the nucleotides that flank the binding site (positions 6−30 nt) are sequestered and are unmodified or unreactive. We used *Z*-factor analysis to determine the sequence segments (gray shade) where a statistically significant reduction in reactivity, between the + and −RBP cases, can be observed. These segments span a range $\sim \pm 50$ nts from the position of the binding site, consistent with a previous RNase-based *in vitro* study.[27] In contrast, for the positions spanning the range 70−180 nt, the reactivities for both + and − cases are indistinguishable. Together, the reactivity analysis indicates that the RBP is protecting a wide-swath of RNA, which spans the 5′ UTR, the initiation, and a portion of the elongation region. This protection is alleviated for positions that are distal from the binding site by >50 nts, resulting in a realigned reactivity signature indicating that a similar underlying structure for the RNA molecule is maintained for both reaction conditions.

***In Vivo* SHAPE-seq Measurements Are Consistent with *in Vitro* Measurements.** To confirm the observations of the *in vitro* SHAPE-seq protection footprint, we carried out an *in vivo* SHAPE-seq experiments (see Materials and Methods for differences from the *in vitro* protocol) on the PP7-wt $\delta = 6$ construct at two induction states (Figure 2B): 0 nM of C_4−HSL (blue line, *i.e.*, no PCP-mCerulean present), and 250 nM of C_4−HSL (red line, PCP-mCerulean fully induced). The experiments for both conditions were carried in duplicates on different days. We plot in Figure 2B the reactivity results for both the induced (red) and noninduced (blue) cases. For the noninduced case, we observe a strong reactivity signal (>0.5) over the range spanning −45−110 nts, which diminishes to no reactivity for positions >110. This picture is flipped for the induced case, displaying lower or no reactivity for the −40 to 110 nt range and a sharp increase in reactivity for positions >130 nt. Interestingly, both for the *in vivo* induced and the +RBP *in vitro* cases (orange signals), the region in the signal corresponding to the protein occupied binding site (arrow point down) seems to be slightly more sensitive to modifications in comparison with the adjacent regions. Next, we computed the *Z*-factor for the regions where the differences between the two reactivity signals was statistically significant ($Z > 0$). In the plot, we marked in gray shades the region where the noninduced reactivity was significantly larger than the induced-reactivity. This shaded region flanks the binding site by ∼50 nts both upstream and downstream and is consistent with an interpretation of a wide-swath of PCP protected RNA *in vivo*.

A closer examination of the *in vivo* SHAPE-seq data reveals two major differences from the *in vitro* SHAPE-seq First, the noninduced case generates significantly higher values of reactivity in the −50−110 nt range as compared with the −RBP *in vitro* case. Second, while in the *in vitro* experiments no significant difference was found between the − and +RBP cases over the 80−180 range, in the *in vivo* case a significant difference was observed. In particular, the noninduced signal becomes sharply nonreactive over this range. To gain a structural perspective for the extent of these differences, we plot in Figure 2C two structures. The structures were

DOI: 10.1021/acssynbio.8b00378
ACS Synth. Biol. 2018, 7, 2765−2774

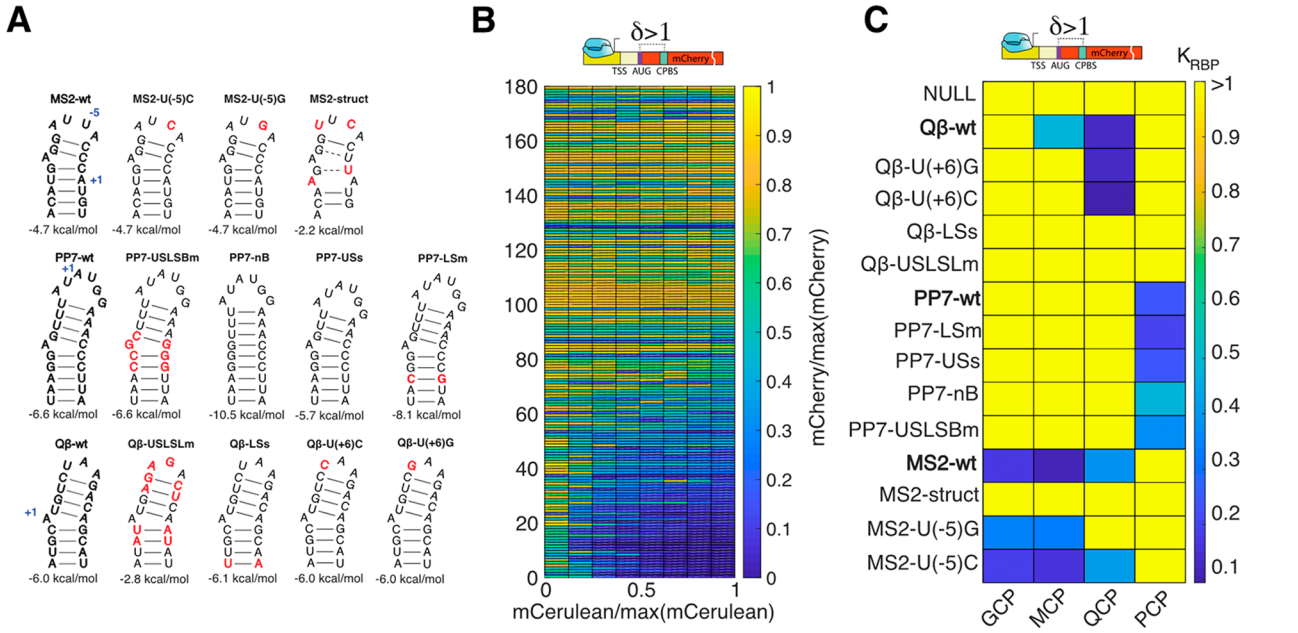

Figure 3. Repression effect can be used to estimate an effective dissociation constant K_{RBP}. (A) Structural schematic for the 14 binding sites used in the binding affinity study. Red nucleotides indicate mutations from the original wt binding sequence. Abbreviations: US/LS/L/B = upper stem/lower stem/loop/bulge, m = mutation, s = short, struct = significant change in binding site structure. (B) Dose responses for 180 variants whose basal rate of production levels were >50 au/h. Each response is divided by its maximal mCherry level, for easier comparison. Variants are arranged in order of increasing fold up-regulation. (C) Normalized K_{RBP} for variants that generated a detectable down-regulatory effect for at least one position. Dark blue corresponds to low K_{RBP}, while yellow indicates high K_{RBP}. If there was no measurable interaction between the RBP and binding site, K_{RBP} was set to 1.

computed using RNAfold[28] for the sequence of this molecule and overlaid by its *in vivo* noninduced (left structure) or induced (right structure) reactivity scores (depicted by a heatmap). We demark the RBS (orange oval), PP7-wt binding site (purple oval), and the putative RBP-protected region computed *via Z*-factor analysis (gray circle on right structure). The structures reveal that the reactivity for the noninduced case is inconsistent with the structural prediction. This observation is suggestive of a structure-destabilizing role that an initiating 30S subunit may be generating in the 5′UTR and initiation region. A structural role for the ribosome can be further inferred by the complete lack of reactivity observed deeper in the elongation region of the noninduced case, which is consistent with the presence of a chain of translating ribosomes that may be protecting the RNA from modifications. This is supported by the recovery of the reactivity signal in the elongation region for the induced case, where translation is for the most part abolished. Consequently, the SHAPE-seq analysis *in vivo* reveals significant structural differences between the induced and noninduced cases that are consistent with their RBP-bound states, resultant translational level, and the observed post-transcriptional repression.

Effective Dissociation Constant of RBPs Is Insensitive to Binding-Site Position. Given the strong RBP-induced repression phenomenon observed for the $\delta < 15$ region, we hypothesized that we can use this effect to further characterize the binding of the RBPs to structured binding sites. To do so, we constructed a set of mutated binding sites with various structure-modifying and nonstructure-modifying mutations [compare Figure 3A: bold letters highlighting the native sites for MCP (MS2-wt, top-left), PCP (PP7-wt, middle-left), and QCP (Qβ-wt, bottom-left)]. The mutated binding sites for MCP and PCP were taken from refs 29, 30, and 18, respectively (Figure 3A), while the ones for QCP were devised by us. All mutations are highlighted in red letters. We then constructed two to four new constructs for each mutated binding site that differed in binding-site position downstream to the AUG. In addition, we constructed a set of control plasmids that lacked a hairpin within the N-terminus of the mCherry reporter gene. Altogether, we constructed 27 additional hairpin-reporter plasmids and 10 no-hairpin controls (see Table S1). The new constructs, and the ones previously tested (Figure 1B, 61 in total), were cotransformed with all four RBP plasmids to yield 232 RBP−binding site strains (*i.e.*, not all potential binding site−RBP pairs were covered). Our goal with this design was to test not only the binding affinity to the native RBPs, but also the relative affinity to the other RBPs, thus obtaining an estimate for the selectivity of RBP binding.

We plot the dose−response curves of 180 out of the 232 strains as a heatmap in Figure 3B (strains with basal mCherry rate of production <50 au/h were excluded). In all cases, the data for both the mCherry rate of production and mean mCerulean levels are normalized by the respective maximal value. The dose response functions are arranged in accordance with fold-regulation of the response, with the most repressive variants positioned at the bottom, and the least repressive at the top. The data show that there is a substantial subset of strains, which exhibit strong repression for at least one hairpin position (~50 variants), with the strongest mCherry signal occurring at the lowest mCerulean level. To obtain an estimate for the effective binding affinity for each down-regulating variant, we fitted each dose−response curve that exhibited a typical repression response (see Figure S1) with a Hill-function-based model (see Supporting Methods), which assumes a simple relationship between the concentration of RBP measured by its fluorescence, the dissociation constant,

DOI: 10.1021/acssynbio.8b00378
ACS Synth. Biol. 2018, 7, 2765−2774

and the output expression rate. Finally, we normalized the resulting dissociation constant by the maximal mCerulean expression for the matching RBP to facilitate comparison of the results for the different proteins, yielding an effective dissociation constant (K_{RBP}, see Table S5). Typical error in estimation of the effective dissociation constant was 5−20%, and by averaging K_{RBP} of each RBP−binding site pair over multiple positions (values of δ) we obtained estimated errors of ∼10%.

In Figure 3C, we plot the averaged K_{RBP} for different RBP−binding site combinations as a heatmap, only for those sites (Figure 3A) for which all four RBPs were tested ("null" corresponds to an average K_{RBP} computation made on several of the non-binding-site controls). The data show that the effective dissociation constants measured for native sites with their cognate RBPs were low and approximately equal, indicating that native sites are evolutionarily optimized for binding (blue squares). Mutated sites which retained binding affinity displayed slightly larger dissociation constants (light-blue/turquoise), while the K_{RBP} values of RBP-binding site combinations that did not generate a binding signature were set to the maximum normalized value 1 (K_{RBP} > 1, yellow). When examining the data more closely, we found that PCP is completely orthogonal to the MCP/QCP/GCP group, with no common binding sites. Conversely, we observed crosstalk between the different members of the MCP/QCP/GCP group, with increased overlap between MCP and GCP, which is consistent with previous studies.[16]

A closer look at the mutant binding sites reveals that structure-conserving mutations to native binding sites in the loop area [Qβ-U(+6)G, Qβ-U(+6)C, MS2-U(−5)C and MS2-U(−5)G] or stem (PP7-USLSBm and PP7-LSs) did not seem to affect binding of the cognate protein. However, the interaction with a noncognate RBP is either diminished or eliminated altogether as is the case for MCP with Qβ-U(+6)G and Qβ-U(+6)C, and for QCP with MS2-U(−5)G. In addition, putative structure-altering (MS2-struct, where the lower stem is abolished) and destabilizing (Qb-USLSLm, where the GC base-pairs are converted to UA base pairs in the lower stem) mutations significantly affected binding. Finally, structure-altering mutations, which retain apparent binding site stability (PP7-nB and PP7-USs), also seemed to retain at least a partial binding affinity to the native RBP. Altogether, these results suggest that binding sites positioned within the δ < 15 nt region can tolerate multiple mutations as long as certain key structural features necessary for binding and hairpin stability (*e.g.*, loop size) are conserved, as was previously observed *in vitro*.[18,30−32]

DISCUSSION

Synthetic biology approaches have been increasingly used in recent years to map potential regulatory mechanisms of transcriptional and translational regulation, in both eukaryotic and bacterial cells. In this work, we built on the work of ref 13 to design a hybrid transcriptional and post-transcriptional regulatory circuit to quantitatively study RBP-based regulation in bacteria using a combined synthetic biology and SHAPE-seq approach. Using our library of RNA regulatory variants, we were able to identify and characterize a position-dependent repression of translation when the hairpin was bound by an RBP. The extent of the repression effect was strongly dependent on position, and diminished for δ > 15. The localization of a strong inhibition effect to region nearby the AUG for at least two different RBP-hairpin pairs suggests that this region may be particularly susceptible for repression effects. Previous works[33,34] have provided evidence that the ribosomal initiation region extends from the RBS to about 9−11 nucleotides downstream of the AUG (δ = 12 to δ = 14 as in our coordinate system). Furthermore, these authors also showed that structured stems of 6 bp or longer in the N-terminus can silence expression up to +11−13 from the AUG, but show negligible silencing when positioned further downstream. Thus, the region where the strong regulatory effects were detected in our experiments likely overlaps with the presumed ribosomal initiation region. This suggests that translation initiation may be susceptible to regulation, which can be an important guideline for RNA-based synthetic biology circuit design.

The sensitivity of the initiation region to translation regulation is further supported by SHAPE-seq reactivity analysis using both a signal-to-noise and a model-based approach. For both *in vitro* and *in vivo* experiments, the analysis revealed that the RBP-binding effect spanned a much wider segment of RNA than previously reported both for phage coat proteins *in vitro*[27] and for other proteins with their cognate RNA target using SHAPE-MaP.[22] There are several scenarios, which may explain this result. In one scenario, PCP may form a large multiprotein complex that is anchored to the binding site, which in turn can lead to a wide protected segment on the RNA. Such a scenario can stem from the capsid-forming characteristics of PCP, even though *PCP-delF-G* was the version used in all experiments, which lack the component that is associated with multidimerization. Alternatively, PCP binding may trigger refolding of flanking regions to form structures with fewer noninteracting nucleotides leading to the reduced reactivity result in those regions in the *in vitro* setting. In the *in vivo* setting a cascade of structural events may be triggered by the refolding or protection of the flanking segments in the immediate vicinity of the binding site. Since these segments include the ribosome binding site, any protection or structuring effect is likely to inhibit initiation and subsequent elongation. This will make the mRNA devoid of ribosomes, which will in turn lead to restructuring of mRNA segments further away from the hairpin resulting in the translationally inactive and highly structured induced state inferred from the reactivity data.

The strong fold repression effect generated by the RBP within the initiation region allowed us to characterize the specific *in vivo* interaction of each RBP−binding site pair by an effective K_{RBP}, which we found to be independent of binding site location. Interestingly, the *in vivo* K_{RBP} measured for some of the binding sites relative to their native site, differ from past *in vitro* and *in situ* measurements. In particular, PP7-nB,PP7-USs, and MS2-U(−5)G exhibited little or no binding in the *in vitro* setting,[18,30] yet displayed strong binding in our assay, while MS2-U(−5)C exhibited a reverse behavior—very high affinity *in vitro* and lower affinity in our assay.[30] Finally, MS2-struct showed no binding in our assay, but exhibited an affinity higher to that of the wild type in an *in situ* setting.[29] These discrepancies may be due to structural constraints, as our *in vivo* RNA constructs were significantly longer than what was used previously *in vitro* and included a 700 nt reporter gene. Another reason for these differences may stem from variations in structure of RNA molecules that emerges from their presence inside cells. Our SHAPE-seq analysis revealed that for at least the one construct that was characterized, a transla-

DOI: 10.1021/acssynbio.8b00378
ACS Synth. Biol. 2018, 7, 2765−2774

tionally active mRNA molecule is less structured *in vivo* as compared with its counterpart *in vitro*. This phenomenon was also previously observed in other studies.[35−37] Such structural differences may lead to intramolecular interactions that yield stable folded states *in vivo* that are more amenable to binding as compared with the short constructs that were used in the *in vitro* experiment, and vice versa.

Finally, we found that both MCP and QCP can bind binding sites with different loop sizes than the wild-type binding sites with relatively high affinity. While they do not seem to be sensitive to the sequence content for a loop whose size is equal to the cognate loop (*i.e.*, 4 nt for MCP and 3 nt for QCP), sequence sensitivity is observed for noncognate loop sizes for both RBPs. This implies that either [GCP, QCP, and PCP] or [MCP, QCP, and PCP], are capable of binding mutually orthogonal binding sites that differ in structure, opening the door for smart design of mutated binding sites for applications where either set of the three RBPs can be used simultaneously. Our work thus establishes a blueprint for an *in vivo* assay for measuring the dissociation constant of RBPs with respect to their candidate binding sites in a more natural *in vivo* setting. This assay can be used to discover additional binding sites for known RBPs, which could be utilized in synthetic biology applications where multiple nonidentical or orthogonal binding sites are needed.

MATERIALS AND METHODS

Design and Construction of Binding-Site Plasmids. Binding-site cassettes (see Table S1) were ordered either as double-stranded DNA minigenes from Gen9 or as cloned plasmids (minigene + vector) from Twist Biosciences. Each minigene was ∼500 bp long and contained the parts in the following order: EagI restriction site, ∼40 bases of the 5′ end of the Kanamycin (Kan) resistance gene, pLac-Ara promoter, ribosome binding site (RBS), an RBP binding site, 80 bases of the 5′ end of the mCherry gene, and an ApaLI restriction site. As mentioned, each cassette contained either a wild-type or a mutated RBP binding site (see Table S1), at varying distances downstream to the RBS. All binding sites were derived from the wild-type binding sites of the coat proteins of one of the four bacteriophages MS2, PP7, GA and Qβ. For insertion into the binding-site plasmid backbone, they were double-digested with EagI-HF and ApaLI (New England Biolabs [NEB]). The digested minigenes were then cloned into the binding-site backbone containing the rest of the mCherry gene, terminator, and a Kanamycin resistance gene, by ligation and transformation into *E. coli* TOP10 cells (ThermoFisher Scientific). Purified plasmids were stored in 96-well format, for transformation into *E. coli* TOP10 cells containing one of four fusion-RBP plasmids (see below).

Design and Construction of Fusion-RBP Plasmids. RBP sequences lacking a stop codon were amplified *via* PCR of either Addgene or custom-ordered templates (Genescript or IDT, see Table S2). All RBPs presented (MCP, PCP, GCP, and QCP) were cloned into the RBP plasmid between restriction sites *Kpn*I and AgeI, immediately upstream of an mCerulean gene lacking a start codon, under the pRhlR promoter (containing the *rhlAB* las box[38]) and induced by C_4−HSL. The backbone contained an Ampicillin (Amp) resistance gene. The resulting fusion-RBP plasmids were transformed into *E. coli* TOP10 cells. After Sanger sequencing, positive transformants were made chemically competent and stored at −80 °C in 96-well format.

Transformation of Binding-Site Plasmids. Binding-site plasmids stored in a 96-well format were simultaneously transformed into chemically competent bacterial cells containing one of the RBP-mCeulean plasmids. After transformation, cells were plated using an 8-channel pipettor on 8-lane plates (Axygen) containing LB-agar with relevant antibiotics (Kan and Amp). Double transformants were selected, grown overnight, and stored as glycerol stocks at −80 °C in 96-well plates (Axygen).

RNA Extraction and Reverse-Transcription for qPCR Measurements. Starters of *E. coli* TOP10 containing the relevant constructs on plasmids were grown in LB medium with appropriate antibiotics overnight (16 h). The next morning, the cultures were diluted 1:100 into fresh semipoor medium and grown for 5 h. For each isolation, RNA was extracted from 1.8 mL of cell culture using standard protocols. Briefly, cells were lysed using Max Bacterial Enhancement Reagent followed by TRIzol treatment (both from Life Technologies). Phase separation was performed using chloroform. RNA was precipitated from the aqueous phase using isopropanol and ethanol washes, and then resuspended in RNase-free water. RNA quality was assessed by running 500 ng on 1% agarose gel. After extraction, RNA was subjected to DNase (Ambion/Life Technologies) and then reverse-transcribed using MultiScribe Reverse Transcriptase and random primer mix (Applied Biosystems/Life Technologies). For qPCR experiments, RNA was isolated from three individual colonies for each construct.

qPCR Measurements. Primer pairs for mCherry and normalizing gene *idnT* were chosen using the Primer Express software and aligned using BLAST[39] (NCBI) with respect to the *E. coli* K-12 substr. DH10B (taxid:316385) genome (which is similar to TOP10) to avoid off-target amplicons. qPCR was carried out on a QuantStudio 12K Flex machine (Applied Biosystems/Life Technologies) using SYBR-Green. Three technical replicates were measured for each of the three biological replicates. A C_T threshold of 0.2 was chosen for all genes.

***In Vivo* SHAPE-seq.** LB medium supplemented with appropriate concentrations of Amp and Kan was inoculated with glycerol stocks of bacterial strains harboring both the binding-site plasmid and the RBP-fusion plasmid (see Table S3 for details of primers and barcodes, and Figure S2), and grown at 37 °C for 16 h while shaking at 250 rpm. Overnight cultures were diluted 1:100 into semipoor medium. Each bacterial sample was divided into a noninduced sample and an induced sample in which RBP protein expression was induced with 250 nM *N*-butanoyl-L-homoserine lactone (C_4−HSL), as described above.

Bacterial cells were grown until OD_{600} = 0.3, 2 mL of cells were centrifuged and gently resuspended in 0.5 mL semipoor medium supplemented with a final concentration of 30 mM 2-methylnicotinic acid imidazole (NAI) suspended in anhydrous dimethyl sulfoxide (DMSO, Sigma-Aldrich),[6,14] or 5% (v/v) DMSO. Cells were incubated for 5 min at 37 °C while shaking and subsequently centrifuged at 6000*g* for 5 min. Column-based RNA isolation (RNeasy mini kit, QIAGEN) was performed for the strain harboring PP7-wt δ = 6. Samples were divided into the following subsamples (Figure S2A):

1. induced/modified (+C_4−HSL/+NAI)
2. noninduced/modified (−C_4−HSL/+NAI)
3. induced/nonmodified (+C_4−HSL/+DMSO)

DOI: 10.1021/acssynbio.8b00378
ACS Synth. Biol. 2018, 7, 2765−2774

4. noninduced/nonmodified (−C_4−HSL/+DMSO).

Subsequent steps of the SHAPE-seq protocol, that were applied to all samples, have been described elsewhere,[15] including reverse transcription (steps 40−51), adapter ligation and purification (steps 52−57) as well as dsDNA sequencing library preparation (steps 68−76). In brief, 1000 ng of RNA were converted to cDNA using the reverse transcription primers (for details of primer and adapter sequences used in this work see Table S3). The RNA was mixed with 0.5 μM primer for mCherry (#1) and incubated at 95 °C for 2 min followed by an incubation at 65 °C for 5 min. The Superscript III reaction mix (Thermo Fisher Scientific; 1× SSIII First Strand Buffer, 5 mM DTT, 0.5 mM dNTPs, 200 U Superscript III reverse transcriptase) was added to the cDNA/primer mix, cooled down to 45 °C and subsequently incubated at 52 °C for 25 min. Following inactivation of the reverse transcriptase for 5 min at 65 °C, the RNA was hydrolyzed (0.5 M NaOH, 95 °C, 5 min) and neutralized (0.2 M HCl). cDNA was precipitated with 3 volumes of ice-cold 100% ethanol, incubated at −80 °C for 15 min, centrifuged at 4 °C for 15 min at 17 000*g* and resuspended in 22.5 μL ultrapure water. Next, 1.7 μM of 5′ phosphorylated ssDNA adapter (#2) (see Table S3) was ligated to the cDNA using a CircLigase (Epicenter) reaction mix (1× CircLigase reaction buffer, 2.5 mM $MnCl_2$, 50 μM ATP, 100 Units CircLigase). Samples were incubated at 60 °C for 120 min, followed by an inactivation step at 80 °C for 10 min cDNA was ethanol precipitated (3 volumes ice-cold 100% ethanol, 75 mM sodium acetate [pH 5.5], 0.05 mg/mL glycogen [Invitrogen]). After an overnight incubation at −80 °C, the cDNA was centrifuged (4 °C, 30 min at 17 000g) and resuspended in 20 μL ultrapure water. To remove nonligated adapter (#2), resuspended cDNA was further purified using the Agencourt AMPure XP beads (Beackman Coulter) by mixing 1.8× of AMPure bead slurry with the cDNA and incubation at room temperature for 5 min. The subsequent steps were carried out with a DynaMag-96 Side Magnet (Thermo Fisher Scientific) according to the manufacturer's protocol. Following the washing steps with 70% ethanol, cDNA was resuspended in 20 μL ultrapure water. cDNAs were subjected to PCR amplification to construct dsDNA library as detailed below.

RBP Protection Assay Using *in Vitro* SHAPE-seq. *In vitro* modification was carried out on noninduced, DMSO-treated samples (Figure S3A) and has been described elsewhere.[6] Briefly, 1500 ng of isolated RNA were denatured at 95 °C for 5 min, transferred to ice for 1 min and incubated in SHAPE-seq reaction buffer (100 mM HEPES [pH 7.5], 20 mM $MgCl_2$, 6.6 mM NaCl) supplemented with 40 U of RiboLock RNase inhibitor (Thermo Fisher Scientific) for 5 min at 37 °C allowing the RNA molecule to refold. Next, we added 15.6 pmol (based on 1:2 molar ratio between RNA:PP7 protein) of highly purified recombinant PP7 protein (Genscript) to the RNA samples and incubated at 37 °C for 30 min. Subsequently, final concentrations of 100 mM NAI or 5% (v/v) DMSO were added to the RNA-PP7 protein reaction mix and incubated for an additional 10 min at 37 °C. Samples were then transferred to ice to stop the SHAPE reaction and precipitated by addition of 300 μL ice-cold 100% ethanol, 10 μL Sodium Acetate 3M, 0.5 μL ultrapure glycogen (Thermo scientific) and 70 μL DEPC-treated water. Samples were incubated at −80 °C for 15 min followed by centrifugation at 4 °C, 17 000*g* for 15 min. Supernatant was removed and samples were air-dried for 5 min at room temperature and resuspended in 10 μL of RNase-free water.

SHAPE-Seq Library Preparation and Sequencing. To produce the dsDNA for sequencing 10 μL of purified cDNA from the SHAPE procedure (see above) were PCR amplified using 3 primers: 4 nM mCherry selection (#3) (primer extends 4 nucleotides into mCherry transcript to avoid the enrichment of ssDNA-adapter products), 0.5 μM TruSeq Universal Adapter (#4) and 0.5 μM TrueSeq Illumina indexes (one of #5−16) (Table S3) with PCR reaction mix (1× Q5 HotStart reaction buffer, 0.1 mM dNTPs, 1 U Q5 HotStart Polymerase [NEB]). A 15-cycle PCR program was used: initial denaturation at 98 °C for 30 s followed by a denaturation step at 98 °C for 15 s, primer annealing at 65 °C for 30 s and extension at 72 °C for 30 s, followed by a final extension 72 °C for 5 min. Samples were chilled at 4 °C for 5 min. After cool-down, 5 U of Exonuclease I (ExoI, NEB) were added, incubated at 37 °C for 30 min followed by mixing 1.8× volume of Agencourt AMPure XP beads to the PCR/ExoI mix and purified according to manufacturer's protocol. Samples were eluted in 20 μL ultrapure water. After library preparation, samples were analyzed using the TapeStation 2200 DNA ScreenTape assay (Agilent) and the molarity of each library was determined by the average size of the peak maxima and the concentrations obtained from the Qubit fluorimeter (Thermo Fisher Scientific). Libraries were multiplexed by mixing the same molar concentration (2−5 nM) of each sample library and sequenced using the Illumina HiSeq 2500 sequencing system using 2 × 100 bp paired-end reads.

Analysis Routines and Models. See the Supporting Information.

■ ASSOCIATED CONTENT

Supporting Information

The Supporting Information is available free of charge on the ACS Publications website at DOI: 10.1021/acssynbio.8b00378.

Detailed modeling and analysis routines, Figures S1−S4 (PDF)
Table S1 (XLSX)
Table S2 (XLSX)
Table S3 (XLSX)
Table S4 (XLSX)
Table S5 (XLSX)

■ AUTHOR INFORMATION

Corresponding Author

*Tel: 972-77-8871894. Fax: 972-4-8293399. E-mail: roeeamit@technion.ac.il.

ORCID

Roee Amit: 0000-0003-0580-7076

Author Contributions

#N.K. and R.C. contributed equally.

Notes

The authors declare no competing financial interest.

■ ACKNOWLEDGMENTS

The authors would like to acknowledge the Technion's LS&E staff (Tal Katz-Ezov and Anastasia Diviatis) for help with sequencing of the SHAPE-seq fragments. This project received funding the I-CORE Program of the Planning and Budgeting

DOI: 10.1021/acssynbio.8b00378
ACS Synth. Biol. 2018, 7, 2765−2774

Committee and the Israel Science Foundation (Grant No. 152/11), Marie Curie Reintegration Grant No. PCIG11-GA-2012-321675, and by the European Union's Horizon 2020 Research And Innovation Programme under Grant Agreement No. 664918 - MRG-Grammar.

REFERENCES

(1) Cerretti, D. P., Mattheakis, L. C., Kearney, K. R., Vu, L., and Nomura, M. (1988) Translational regulation of the spc operon in Escherichia coli. *J. Mol. Biol. 204*, 309−325.

(2) Sacerdot, C., Caillet, J., Graffe, M., Eyermann, F., Ehresmann, B., Ehresmann, C., Springer, M., and Romby, P. (1998) The Escherichia coli threonyl-tRNA synthetase gene contains a split ribosomal binding site interrupted by a hairpin structure that is essential for autoregulation. *Mol. Microbiol. 29*, 1077−1090.

(3) Lucks, J. B., Mortimer, S. A., Trapnell, C., Luo, S., Aviran, S., Schroth, G. P., Pachter, L., Doudna, J. A., and Arkin, A. P. (2011) Multiplexed RNA structure characterization with selective 2′-hydroxyl acylation analyzed by primer extension sequencing (SHAPE-Seq). *Proc. Natl. Acad. Sci. U. S. A. 108*, 11063−11068.

(4) Rouskin, S., Zubradt, M., Washietl, S., Kellis, M., and Weissman, J. S. (2014) Genome-wide probing of RNA structure reveals active unfolding of mRNA structures in vivo. *Nature 505*, 701−705.

(5) Ding, Y., Kwok, C. K., Tang, Y., Bevilacqua, P. C., and Assmann, S. M. (2015) Genome-wide profiling of in vivo RNA structure at single-nucleotide resolution using structure-seq. *Nat. Protoc. 10*, 1050−1066.

(6) Flynn, R. A., Zhang, Q. C., Spitale, R. C., Lee, B., Mumbach, M. R., and Chang, H. Y. (2016) Transcriptome-wide interrogation of RNA secondary structure in living cells with icSHAPE. *Nat. Protoc. 11*, 273−290.

(7) Zubradt, M., Gupta, P., Persad, S., Lambowitz, A. M., Weissman, J. S., and Rouskin, S. (2017) DMS-MaPseq for genome-wide or targeted RNA structure probing in vivo. *Nat. Methods 14*, 75−82.

(8) Kinney, J. B., Murugan, A., Callan, C. G., and Cox, E. C. (2010) Using deep sequencing to characterize the biophysical mechanism of a transcriptional regulatory sequence. *Proc. Natl. Acad. Sci. U. S. A. 107*, 9158−9163.

(9) Sharon, E., Kalma, Y., Sharp, A., Raveh-Sadka, T., Levo, M., Zeevi, D., Keren, L., Yakhini, Z., Weinberger, A., and Segal, E. (2012) Inferring gene regulatory logic from high-throughput measurements of thousands of systematically designed promoters. *Nat. Biotechnol. 30*, 521−530.

(10) Patwardhan, R. P., Hiatt, J. B., Witten, D. M., Kim, M. J., Smith, R. P., May, D., Lee, C., Andrie, J. M., Lee, S.-I., Cooper, G. M., et al. (2012) Massively parallel functional dissection of mammalian enhancers in vivo. *Nat. Biotechnol. 30*, 265−270.

(11) Levy, L., Anavy, L., Solomon, O., Cohen, R., Brunwasser-Meirom, M., Ohayon, S., Atar, O., Goldberg, S., Yakhini, Z., and Amit, R. (2017) A Synthetic Oligo Library and Sequencing Approach Reveals an Insulation Mechanism Encoded within Bacterial σ54Promoters. *Cell Rep. 21*, 845−858.

(12) Weingarten-Gabbay, S., Elias-Kirma, S., Nir, R., Gritsenko, A. A., Stern-Ginossar, N., Yakhini, Z., Weinberger, A., and Segal, E. (2016) Comparative genetics. Systematic discovery of cap-independent translation sequences in human and viral genomes. *Science 351*, aad4939.

(13) Saito, H., Kobayashi, T., Hara, T., Fujita, Y., Hayashi, K., Furushima, R., and Inoue, T. (2010) Synthetic translational regulation by an L7Ae−kink-turn RNP switch. *Nat. Chem. Biol. 6*, 71−78.

(14) Spitale, R. C., Crisalli, P., Flynn, R. A., Torre, E. A., Kool, E. T., and Chang, H. Y. (2013) RNA SHAPE analysis in living cells. *Nat. Chem. Biol. 9*, 18−20.

(15) Watters, K. E., Abbott, T. R., and Lucks, J. B. (2016) Simultaneous characterization of cellular RNA structure and function with in-cell SHAPE-Seq. *Nucleic Acids Res. 44*, No. e12.

(16) Gott, J. M., Wilhelm, L. J., and Uhlenbeck, O. C. (1991) RNA binding properties of the coat protein from bacteriophage GA. *Nucleic Acids Res. 19*, 6499−6503.

(17) Peabody, D. S. (1993) The RNA binding site of bacteriophage MS2 coat protein. *EMBO J. 12*, 595−600.

(18) Lim, F., and Peabody, D. S. (2002) RNA recognition site of PP7 coat protein. *Nucleic Acids Res. 30*, 4138−4144.

(19) Lim, F., Spingola, M., and Peabody, D. S. (1996) The RNA-Binding Site of Bacteriophage Qβ Coat Protein. *J. Biol. Chem. 271*, 31839−31845.

(20) Zeevi, D., Sharon, E., Lotan-Pompan, M., Lubling, Y., Shipony, Z., Raveh-Sadka, T., Keren, L., Levo, M., Weinberger, A., and Segal, E. (2011) Compensation for differences in gene copy number among yeast ribosomal proteins is encoded within their promoters. *Genome Res. 21*, 2114−2128.

(21) Keren, L., Zackay, O., Lotan-Pompan, M., Barenholz, U., Dekel, E., Sasson, V., Aidelberg, G., Bren, A., Zeevi, D., Weinberger, A., et al. (2013) Promoters maintain their relative activity levels under different growth conditions. *Mol. Syst. Biol. 9*, 701.

(22) Smola, M. J., Calabrese, J. M., and Weeks, K. M. (2015) Detection of RNA-Protein Interactions in Living Cells with SHAPE. *Biochemistry 54*, 6867−6875.

(23) Choudhary, K., Ruan, L., Deng, F., Shih, N., and Aviran, S. (2016) SEQualyzer: interactive tool for quality control and exploratory analysis of high-throughput RNA structural profiling data. *Bioinformatics 33*, btw627.

(24) Aviran, S., Lucks, J. B., and Pachter, L. (2011) RNA structure characterization from chemical mapping experiments. In *2011 49th Annual Allerton Conference on Communication, Control, and Computing (Allerton)*, pp 1743−1750, IEEE.

(25) Zhang, J.-H., and Chung and Oldenburg (1999) A Simple Statistical Parameter for Use in Evaluation and Validation of High Throughput Screening Assays. *J. Biomol. Screening 4*, 67−73.

(26) Siegfried, N. A., Busan, S., Rice, G. M., Nelson, J. A. E., and Weeks, K. M. (2014) RNA motif discovery by SHAPE and mutational profiling (SHAPE-MaP). *Nat. Methods 11*, 959−965.

(27) Bernardi, A., and Spahr, P.-F. (1972) Nucleotide Sequence at the Binding Site for Coat Protein on RNA of Bacteriophage R17. *Proc. Natl. Acad. Sci. U. S. A. 69*, 3033−3037.

(28) Hofacker, I. L., Fontana, W., Stadler, P. F., Bonhoeffer, S., Tacker, M., and Schuster, P. (1994) Fast folding and comparison of RNA secondary structures. *Monatsh. Chem. 125*, 167−188.

(29) Buenrostro, J. D., Araya, C. L., Chircus, L. M., Layton, C. J., Chang, H. Y., Snyder, M. P., and Greenleaf, W. J. (2014) Quantitative analysis of RNA-protein interactions on a massively parallel array reveals biophysical and evolutionary landscapes. *Nat. Biotechnol. 32*, 562−568.

(30) Johansson, H. E., Dertinger, D., LeCuyer, K. A., Behlen, L. S., Greef, C. H., and Uhlenbeck, O. C. (1998) A thermodynamic analysis of the sequence-specific binding of RNA by bacteriophage MS2 coat protein. *Proc. Natl. Acad. Sci. U. S. A. 95*, 9244−9249.

(31) Spingola, M., and Peabody, D. S. (1997) MS2 coat protein mutants which bind Qbeta RNA. *Nucleic Acids Res. 25*, 2808−2815.

(32) Witherell, G. W., and Uhlenbeck, O. C. (1989) Specific RNA binding by Q.beta. coat protein. *Biochemistry 28*, 71−76.

(33) Paulus, M., Haslbeck, M., and Watzele, M. (2004) RNA stem−loop enhanced expression of previously non-expressible genes. *Nucleic Acids Res. 32*, No. e78.

(34) Espah Borujeni, A., Cetnar, D., Farasat, I., Smith, A., Lundgren, N., and Salis, H. M. (2017) Precise quantification of translation inhibition by mRNA structures that overlap with the ribosomal footprint in N-terminal coding sequences. *Nucleic Acids Res. 45*, 5437−5448.

(35) Watters, K. E., Yu, A. M., Strobel, E. J., Settle, A. H., and Lucks, J. B. (2016) Characterizing RNA structures in vitro and in vivo with selective 2′-hydroxyl acylation analyzed by primer extension sequencing (SHAPE-Seq). *Methods 103*, 34−48.

DOI: 10.1021/acssynbio.8b00378
ACS Synth. Biol. 2018, 7, 2765−2774

(36) Weissman, J., Rouskin, S., Zubradt, M., Washietl, S., Kellis, M., and Weissman, J. S. (2014) Genome-wide probing of RNA structure reveals active unfolding of mRNA structures in vivo. *Nature 505*, 701.
(37) Ding, Y., Tang, Y., Kwok, C. K., Zhang, Y., C Bevilacqua, P., and M Assmann, S. (2014) In vivo genome-wide profiling of RNA secondary structure reveals novel regulatory features. *Nature 505*, 696.
(38) Medina, G., Juárez, K., Valderrama, B., and Soberón-Chávez, G. (2003) Mechanism of Pseudomonas aeruginosa RhlR Transcriptional Regulation of the rhlAB Promoter. *J. Bacteriol. 185*, 5976−5983.
(39) Altschul, S. F., Gish, W., Miller, W., Myers, E. W., and Lipman, D. J. (1990) Basic local alignment search tool. *J. Mol. Biol. 215*, 403−410.

DOI: 10.1021/acssynbio.8b00378
ACS Synth. Biol. 2018, 7, 2765−2774